

Experimental Study on Passive Scalar Diffusion in a Round Counter Jet by a Combined PIV and PLIF Measurements

H. Tsunoda¹

¹Department of Mechanical Systems Engineering
University of Yamanashi, Takeda 4-3-11, Kofu 400-8511, Japan

Abstract

Simultaneous measurements on the velocity and concentration fields of matter in a turbulent round jet injected into a counter-flowing stream have been conducted by using a combined system of PIV and PLIF techniques. Experiments were carried out for four cases of jet to counter-flow velocity ratios: $V_r = 2.4, 3.4, 5.5$ and 7.8 . Axial profiles of the concentration statistics along the jet centerline showed that both rms concentration fluctuation and streamwise turbulent flux of mass have two peaks in the near field of the jet and in the mean stagnant region. It was also suggested that radial turbulent flux has a tendency to increase in a region where the counter flow deflects radially along the dividing stream line.

Introduction

This paper is concerned with a turbulent jet issuing into external counter flowing stream. Because of its enhanced mixing efficiency in comparison with a round jet in stagnant ambient fluid, this type of flow configuration could be of great importance from fundamental point of view of science as well as from the practical purposes in many engineering applications, especially in environmental, chemical or process engineering.

Figure 1 shows a schematic of the present flow. Earlier works on the counter jet were mainly concerned with a penetration distance, that is, a longitudinal distance from the nozzle exit to the mean stagnation point (e.g. [3] and [7]). Principal difficulties in studying this flow come from its strong instability, depending of the ratio of jet to counter-flow velocities [2]. In a far downstream of the jet exit where the jet is decelerated by the counter-flow, it has been confirmed that the downstream end of the jet fluctuates back and forth over the x -axis and rotates about the axis. These characteristics are believed to be responsible for its mixing enhancement [7]. Recent developments of flow measurement technique have made it possible to tackle these unresolved problems by investigating the dynamical behavior of the jet using digital imaging technology such as Particle Imaging Velocimetry (PIV) or Planar Laser Induced Fluorescence (PLIF).

In applying to combustion or environmental problems, better

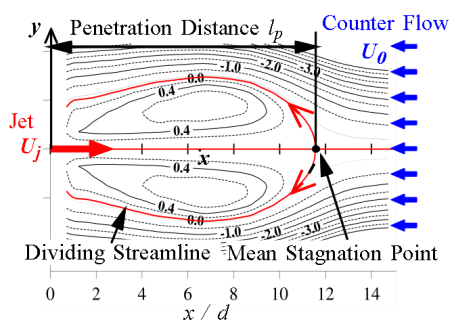


Figure 1 Schematic of flow configuration.

understanding would be required of a scalar diffusion in the counter-jet. Tsunoda and Saruta [5] reported the concentration fields of a passive scalar by using PLIF technique and showed that the rms concentration fluctuation had a noticeable local maximum within the stagnant region. However, no data on the simultaneous statistics, like the correlation between the velocity and concentration fluctuations, were obtained because of their experimental limitation. The present work, therefore, aims to examine the characteristics of the diffusion field of scalar in the counter jet by measuring the velocity and concentration fields simultaneously. Images of both the instantaneous velocity and concentration fields were captured at the same place in the flow field and their correlations were calculated after the data correction based on camera calibration.

Experimental Setup and Conditions

The present experimental apparatus is shown in figure 2. Measurements were carried out in a water channel with 198 mm height, 194 mm width and 2 m long test section. The water depth was kept at 180 mm during the experiment. Circular jet was discharged through a nozzle with exit diameter of $d = 5$ mm into counter-flowing stream with an approximately uniform velocity profile of $U_0 = -0.17$ m/s (in the following, U_0 is defined by its absolute value). The nozzle was placed horizontally at mid-depth of the channel. Four kinds of velocity ratios $V_r = U_j/U_0 = 2.4, 3.4, 5.5$ and 7.8 were adopted in this experiment, where U_j is the jet exit velocity. This was adjusted by changing the height of the head tank and monitored using a turbine flow-meter. The Cartesian coordinate system (x, y) is used such that the origin is located at the center of the nozzle exit and x is the longitudinal coordinate along the jet centerline.

Instantaneous velocity and concentration fields were measured by using PIV and PLIF techniques. The light sheet which originated from a 15 mJ dual-cavity pulsed Nd:YAG laser was supplied vertically through the acrylic bottom-wall of the channel so as to cut through a x - y plane of the flow containing the jet centerline. The jet fluid and the ambient water were seeded by polystyrene particles with an averaged diameter of about $55 \mu\text{m}$.

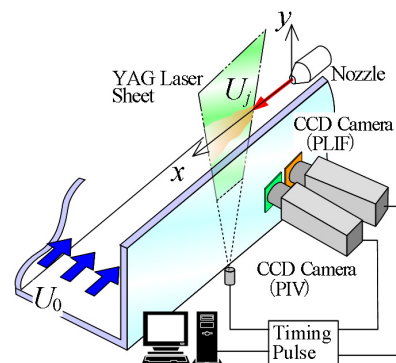


Figure 2 Experimental apparatus and coordinate system.

Furthermore, aqueous solution of Rhodamine 6G with an initial concentration of $C_j = 0.3 \text{ mg/l}$ was discharged from the nozzle as a fluorescent diffusing scalar. The peak emission wavelength of Rhodamine 6G is about 560 nm which is a little longer than that in the incident laser light (532 nm). Two CCD cameras, one for PIV and the other for PLIF were used. In order to isolate the green laser light and the orange fluorescence, a band-pass filter with center wavelength 532 nm and half width 10 nm was attached in front of the PIV camera lens and a high-pass optical filter with cut-off around 540 nm in front of the PLIF camera lens. The PIV camera (Dantec HiSenseMKII, 1344×1024 pixels) was aligned to be perpendicular to the imaged plane, while the camera for PLIF (Dantec DoubleImage 700, 768×484 pixels) was placed at a slightly tilted angle so that the both cameras cover the same area. Since this camera inclination caused an in-negligible amount of the image distortion, camera calibration was conducted in order to eliminate it prior to each experimental run (see [6] on the calibration method). Because of a limited camera resolution, the whole measurement region was divided into several sub-windows depending on the velocity ratios. For example, 18 sub-windows (6×3 images in the directions of x and y , respectively) were adopted for the case of $V_r = 7.8$. Each sub-window size was chosen to be about $42 \times 32 \text{ mm}^2$ for the PIV camera and $44 \times 28 \text{ mm}^2$ for the PLIF camera after the image correction.

Laser illumination and image acquisitions by the two cameras were synchronized by using an external timing-pulse generator which enabled the simultaneous measurement of the velocity and concentration fields. The PIV camera was set to double-frame mode in which two laser pulses from the dual-illumination exposed different frames for the cross-correlation analysis. On the other hand, single-frame mode was adopted for the PLIF camera and two laser pulses, which are the same pulse pair as the PIV illumination, exposed one frame twice. The time duration between pulses was determined according to the PIV requirement. Temporal resolution, that is, the sampling frequency of the PIV image pair of tracers and the PLIF image of fluorescence was fixed to be 5 Hz. Ten sets of 90 consecutive images were captured for the purpose of calculating statistics and thus the total duration of the sampling was 180 s.

Results and discussion

Fundamental Flow Properties

In the first place, fundamental properties of the present flow field are described. The downstream decay of the axial mean velocity U_c along the jet-axis scaled with U_0 is shown in figure 3. At the jet exit U_c/U_0 corresponds to V_r and the x value where U_c is zero (marked by the arrow for each V_r), i.e. the x distance to the mean stagnation point, defines the penetration length l_p . The V_r -dependence of l_p is shown in figure 4. Present data include the past results in author's laboratory and the data by Yoda and Fielder [7] are also included together with approximation lines proposed by Rajaratnam [4]. The present data are approximated well by the expression $l_p/d = 2.4V_r$.

Figure 5 shows the downstream variations of the centerline axial and radial rms velocity fluctuation u'_c and v'_c scaled with U_0 . The abscissa is normalized by l_p . As explained in [5], two peaks exist in the u'_c profiles, independently of V_r . The first is related to the instability of the jet and the second would be explained by an intermittent occurrence of the forward jet-flow and the backward counter-flow around the stagnation point. As contrasted with u'_c , v'_c continues to decay even in the stagnant region.

Concentration Field

Simultaneous images of instantaneous velocity vector and con-

centration field of dyed fluid issued from the nozzle are presented in figure 6 for the case of $V_r = 2.4$. Time interval between two images is 0.2 ms. It can be seen that two instantaneous fields of velocity and concentration are captured satisfactory in the present experiment. Although these are only two examples sampled from 900 images, strong instability in the present counter-jet could be confirmed from two images. The aspect of instantaneous jet penetration into the counter-flow considerably varies around the mean stagnation point and this behavior is related with mixing enhancement of the flow.

Axial variations of the mean concentration C_c and the rms concentration fluctuation c'_c normalized by C_j are shown in figure 7.

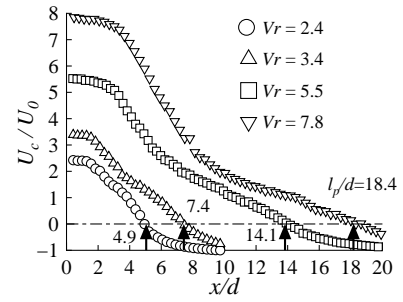


Figure 3 Decay of axial mean velocities U_c on the jet centerline.

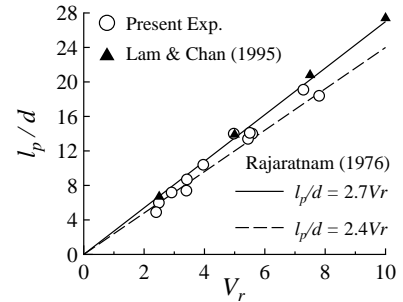


Figure 4 V_r -dependence of penetration distance l_p .

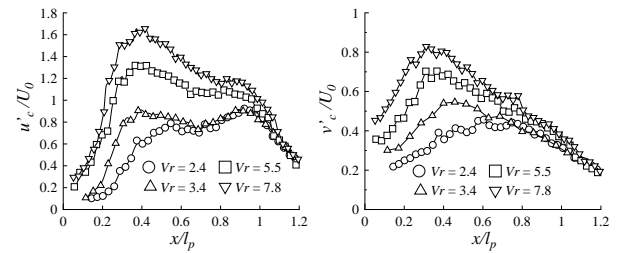


Figure 5 Downstream variations of axial and radial rms velocities on the jet centerline.

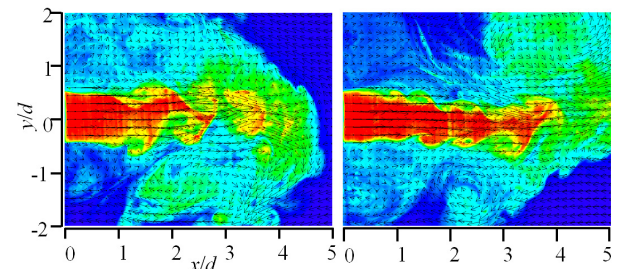


Figure 6 Instantaneous images of velocity vector and concentration field ($V_r = 2.4$). Time interval between figures is 0.2 ms.

Till a mid-distance of l_p ($x/l_p \simeq 0.5 \sim 0.6$) from the exit, the mean concentration decays in a similar way as a conventional jet. Then, after its decay rate once gets slow slightly, it again starts to decay even more rapidly as approaching to the stagnation point. This feature clearly arises from the strong longitudinal and radial wandering of dyed jet fluid near the stagnation point. Some peculiar results also appear in the fluctuating field. The axial profiles of c'_c have double peaks as in the case of the fluctuating velocity field. It can be seen that the magnitude of the second peak decreases with increasing V_r , presumably because of advanced dilution due to longer passage to the stagnant region for larger V_r .

Contour maps of the rms concentration fluctuation c'/C_j are shown in figure 8 for $V_r = 2.4$ and 5.5, together with mean streamlines estimated by assuming the axisymmetric stream function. x is normalized by l_p . Slight distortions in streamlines for $V_r = 5.5$ are considered to be caused by the division of the whole area into several sub-windows as mentioned earlier. It is found from these figures that the local maximum area of c' near the stagnation point extends radially along the dividing streamlines denoted by bold solid line, where the dividing streamline is, on the average, a line separating the jet fluid from the ambient counter-flowing one.

Figure 9 shows axial profiles of the streamwise turbulent mass flux (\overline{uc})_c (i.e. the cross correlation between u -velocity and concentration fluctuations) along the jet centerline. (\overline{uc})_c is normalized by U_0 and C_j . Like u'_c or c'_c on the jet-axis shown in figure 5 and 7, \overline{uc} on the jet axis exhibits two distinct peaks in the near field and in the mean stagnant region of the jet. As increasing V_r , the value of x/l_p attaining the second peak moves to smaller position and the magnitude of the second peak relative to the first decreases.

Contours of the axial and radial turbulent mass flux \overline{uc} and \overline{vc}

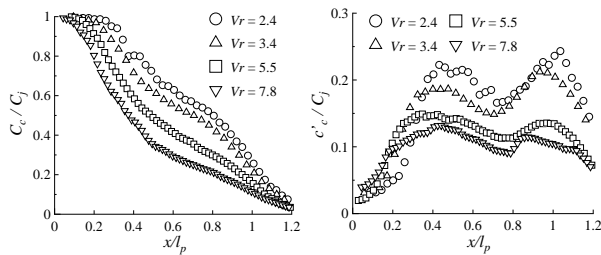


Figure 7 Downstream variations of mean and rms concentration on the jet centerline.

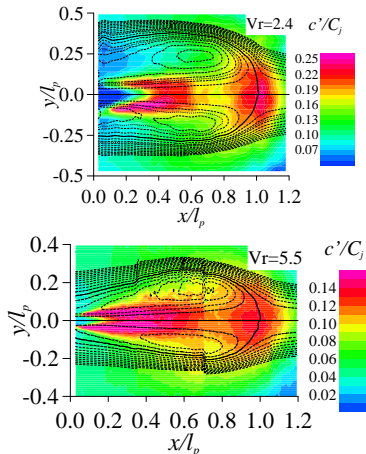


Figure 8 Streamlines and contour map of rms concentration fluctuation (upper: $V_r = 2.4$, lower: $V_r = 5.5$).

scaled by U_0 and C_j are shown in figures 10 and 11 for all V_r cases. It can be seen that \overline{uc} remains positive over the spreading area of the counter-jet and its whole feature is similar with c' shown in figure 8. Within the stagnant region, alternate streamwise transport of dyed fluid in the jet and ambient colorless fluid in the counter-flow could cause this growing in c' and \overline{uc} (see the following on figure 12). Contrasting with \overline{uc} , \overline{vc} increases locally outside the dividing streamline as well as inside the free shear layer, although statistical noise makes this result more or less unclear. The former increase suggests that radial transport of scalar would be mainly caused by a circumferential wandering of the jet about the axis.

To examine the characteristics in \overline{uc} and \overline{vc} , joint probability density functions; P_{uc} between the instantaneous x -directional

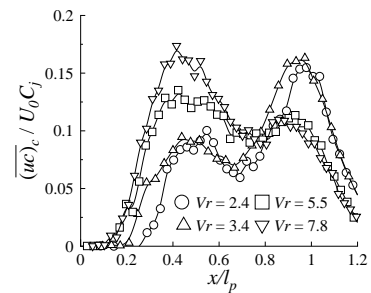


Figure 9 Downstream variations of axial turbulent flux on the jet centerline.

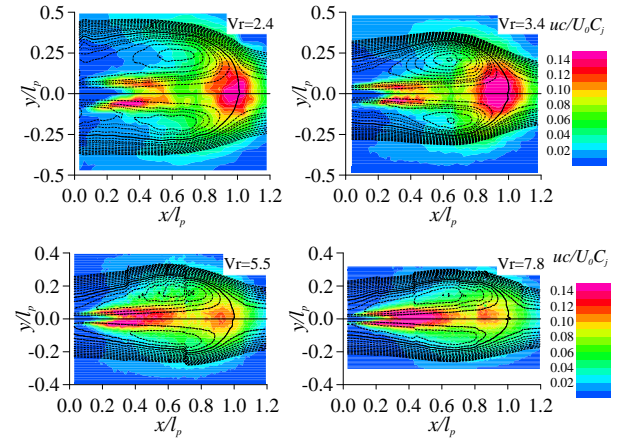


Figure 10 Streamlines and contour map of axial turbulent flux (from upper left, $V_r = 2.4, 3.4, 5.5, 7.8$).

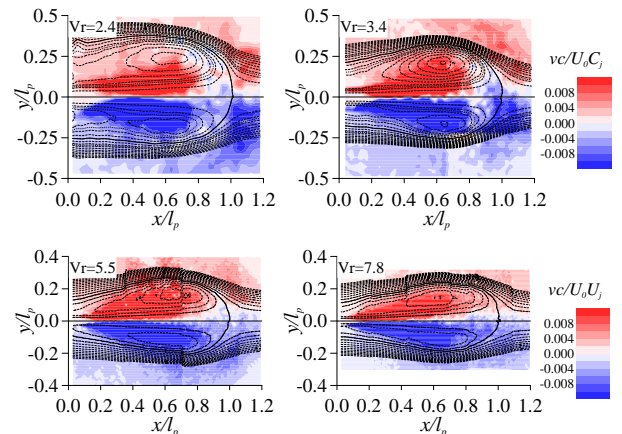


Figure 11 Streamlines and contour map of radial turbulent flux (from upper left, $V_r = 2.4, 3.4, 5.5, 7.8$).

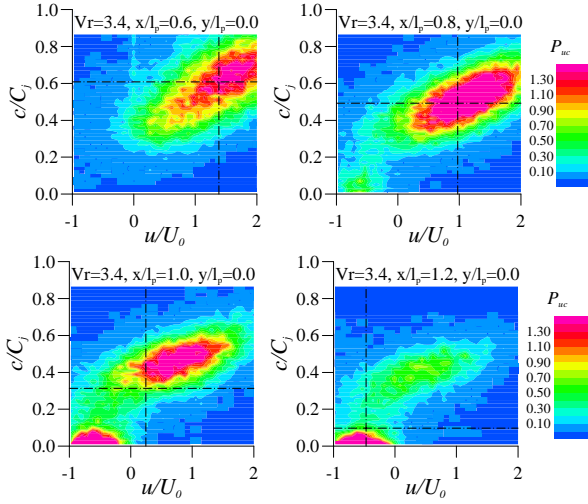


Figure 12 Contours of joint-PDF between u and c for $V_r = 3.4$ on the centerline (from upper left, $x/l_p = 0.6, 0.8, 1.0, 1.2$).

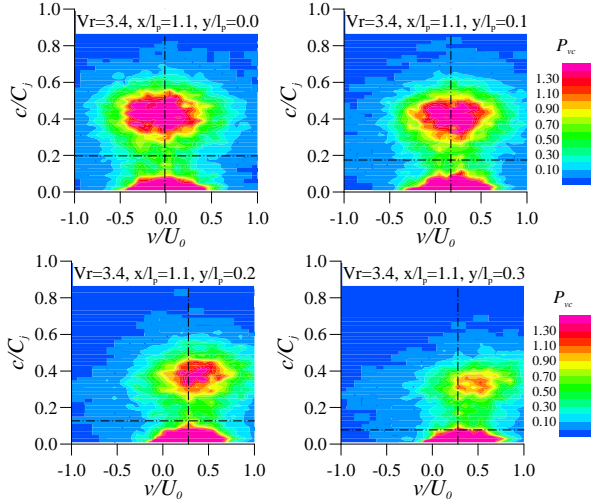


Figure 13 Contours of joint-PDF between v and c for $V_r = 3.4$ at $x/l_p = 1.1$ (from upper left, $y/l_p = 0.0, 0.1, 0.2, 0.3$).

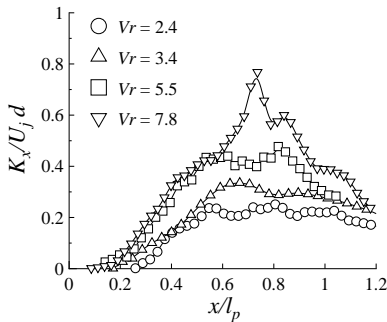


Figure 14 Downstream variations of axial turbulent diffusivity on the jet centerline.

velocity u and concentration c and P_{vc} between the instantaneous y -directional velocity v and c were evaluated near the stagnation point for $V_r = 3.4$. Figure 12 shows the downstream variation of the P_{uc} contour along the centerline and figure 13 the radial variation of the P_{vc} contour at $x/l_p = 1.1$. Mean values for these properties of u , v and c are drawn by the chain lines. At $x/l_p = 0.6$ near which \overline{uc} takes a local minimum, P_{uc} has an elliptic shape whose major axis is inclined in u - c space. As going downstream, it is clearly seen that a region with neg-

ative u and nearly zero concentration starts to appear and thus the joint process of u and c becomes intermittent. Turning to P_{vc} , intermittency appears especially in the concentration field. On the axis P_{vc} is symmetric about the line of $v = 0$ which corresponds to the mean value. For larger y , the symmetry of v field is slowly lost and the fluid lump with higher concentration tends to have a radial velocity larger than the mean value (that is, positive v fluctuation). This tendency can be considered to produce positive \overline{vc} .

By assuming the gradient diffusion, the axial turbulent diffusivity K_x can be estimated by the equation, $K_x = -\overline{uc}/(\partial C/\partial x)$. Downstream variations of K_x on the axis are shown in figure 14, where K_x is scaled by U_j and d . For smaller V_r , K_x becomes nearly constant in a region of $0.6 \lesssim x/l_p \lesssim 1.0$ after an initial jet development. But, as V_r increases the uniformity in K_x is diminished and K_x reaches its peak in an intermediate region from $x/l_p \simeq 0.6$ to 0.8 in relation with C_c -profiles shown in figure 7.

Conclusions

Turbulent diffusion of passive scalar in a round jet penetrating into uniform counter-flow has been examined experimentally. Simultaneous measurements of the velocity and concentration fields by a combined system of PIV and PLIF made it possible to examine essential properties like turbulent mass flux \overline{uc} or \overline{vc} . Streamwise flux \overline{uc} had two distinct peaks along the jet axis; one is in the near field and the other in the mean stagnant region. By investigating the joint PDF between u and c , it was confirmed that alternate streamwise transport of dyed fluid in the jet and ambient fluid in the counter-flow is related with the enhancement in \overline{uc} in the stagnant region. The radial flux \overline{vc} was found to have a tendency to increase in an off-axis area outside the dividing streamline due to a circumferential wandering of the jet about the axis.

Acknowledgements

The funding support from the Japan Society for the Promotion of Science under Grant-in-Aid No. (C)-20560152 is gratefully acknowledged.

References

- [1] Bernero, S. and Fiedler, H.E., Simultaneous PIV and LIF Experiments on a Round Jet in Counterflow, *Proceedings on Turbulence and Shear Flow Phenomena I*, Begell House, 1999, 1053–1058.
- [2] König, O. and Fiedler, H.E., The Structure of Round Turbulent Jets in Counter-flow: A Flow Visualization Study, *Advances in Turbulence 3*, Springer-Verlag Berlin, Heidelberg, 1991, 61–66.
- [3] Lam, K.M. and Chan, H.C., Investigation of Turbulent Jets Issuing into a Counter-flowing Stream Using Digital Image Processing, *Exp. in Fluids*, **18**, 1995, 210–212.
- [4] Rajaratnam, N., *Turbulent Jets*, Elsevier Scien. Publishing, Amsterdam, 1976.
- [5] Tsunoda, H. and Saruta, M., Planar laser-induced fluorescence study on the diffusion field of a round jet in a uniform counter-flow, *Journal of Turbulence*, **4**, 2003, 1–12.
- [6] Tsunoda, H. and Takei, J., Statistical Characteristics of the Cross-Sectional Concentration Field in a Round Counter Jet, *J. of Fluid Sci. and Tech.*, **1**, 2006, 105–113.
- [7] Yoda, M. and Fiedler, H.E., The round jet in a uniform counterflow: flow visualization and mean concentration measurements, *Exp. in Fluids*, **21**, 1996, 427–436.